

# Deep Learning-Based Autoencoder for Data-Driven Modeling of an RF Photoinjector

J. Zhu, Y. Chen, F. Brinker, W. Decking, S. Tomin, H. Schlarb  
*Deutsches Elektronen-Synchrotron DESY, Notkestrasse 85, 22607 Hamburg, Germany*  
(Dated: December 23, 2024)

We adopt a data-driven approach to model the longitudinal phase-space diagnostic beamline at the European XFEL photoinjector. A deep convolutional neural network (decoder) is used to build a 2D distribution from a small feature space learned by another neural network (encoder). We demonstrate that the autoencoder model trained on experimental data can make fast and very high-quality predictions of megapixel images for the longitudinal phase-space measurement. The prediction significantly outperforms existing models. We also show that the knowledge learned by the model can be transferred to speed up training of another model with a different injector setup. This opens the door to a new way of precisely modeling a photoinjector and can be possibly extended to the whole accelerator.

## INTRODUCTION

Operations of large-scale scientific user facilities like European XFEL [1] are very challenging as it is required to meet the specifications of various user experiments [2] and be capable of switching machine status rapidly. Recently, machine learning (ML) is quickly providing new powerful tools for accelerator physicists to build fast-prediction surrogate models [3–5] or extract essential information [6] from large amounts of data. These ML-based models can be extremely useful for accelerator tuning by virtually bringing destructive diagnostics online [4], providing an initial guess of input parameters for a model-independent adaptive feedback control algorithm [7] or driving a model-based feedback control algorithm [8]. One way of training a ML-based model is to use the simulated data. However, beam dynamics simulations are typically carried out under different theoretical assumptions on collective effects such as space charge forces, wakefields and coherent synchrotron radiation. In addition, electron emission from a photocathode is governed by multiple physical processes and is even more difficult to simulate [9]. Moreover, aging of accelerator components affects the long-term operation of a facility, but is generally not included in simulation. As a result, it is extremely challenging to achieve a good agreement between simulation and measurement for a large range of machine operation parameters even exploiting complicated physical models [10]. Furthermore, it can be prohibitively expensive to collect a large amount of high-resolution simulation data [11].

In this letter, we propose a deep learning-based autoencoder to predict high-quality megapixel images on the screen for the longitudinal phase-space measurement using RF phases at the injector of European XFEL. Besides performance, a major advantage of this approach over the existing ones [4, 8] is that the output of our model is the full image from the camera, so that the same neural network structure can be applied on measurements of distributions with different footprints and the pre-processing step is much more simpler. The con-

cerned physical properties can then be extracted by using the well-established routines. Furthermore, existing works tend to use neural networks with no more than five layers [4–6]. We demonstrate that the depth of a neural network is of crucial importance for generating very high-quality predictions.

The general structure of the autoencoder is illustrated in Fig. 1. More generally, given an input  $\mathbf{x} \in \mathbb{R}^m$  and the measurement  $\mathbf{y} \in \mathbb{R}^n$ , the model is asked to learn two neural networks  $g_\varphi : \mathbb{R}^m \rightarrow \mathbb{R}^c$  and  $f_\theta : \mathbb{R}^c \rightarrow \mathbb{R}^n$ , where  $\mathbb{R}^c$  is the latent space and  $\mathbf{z} \in \mathbb{R}^c$  is called latent features. Both  $m$  and  $n$  can be very large as modern area detectors typically have millions of pixels. The learning process is described as minimizing a loss function  $\mathcal{L}(\mathbf{y}, f_\theta(g_\varphi(\mathbf{x})))$  using the gradient descent algorithm. Therefore, the model only learns from non-fixed input data  $\tilde{\mathbf{x}}$  and the encoder can be simplified to  $g_\varphi(\mathbf{x}) = g_\varphi(\tilde{\mathbf{x}}|\bar{\mathbf{x}}) = g_\varphi(\tilde{\mathbf{x}})$ , where  $\bar{\mathbf{x}}$  is the fixed input data and  $\tilde{\mathbf{x}} \oplus \bar{\mathbf{x}} = \mathbf{x}$ . Here we have assumed that the influence of the input jitter is negligible. Although it can be very challenging for neural networks to learn a universal approximator for the whole input parameter space of an accelerator, this approach is well-suited for user facilities as they are typically operated on a finite number of working points. It is worth mentioning that our model is essentially different from the variational autoencoder (VAE) [12] and the generative adversarial network (GAN) [13], both of which learn a joint probability distribution from the training dataset, allowing to synthesize images from random noise.

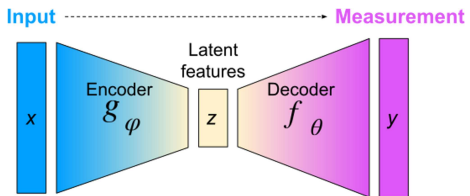


FIG. 1. General architecture of the autoencoder.

Previous work [4] has demonstrated prediction of the longitudinal phase-space at the exit of the LCLS accelerator using a multi-layer perception. The images were

cropped to  $100 \times 100$  pixels and the phase-space distribution must be centered in order to produce good result. However, this requirement limits its application to cases where the distribution has significant different footprints and leads to information loss. In terms of longitudinal phase-space measurement, the absolute energy and longitudinal position of the beam are erased after this pre-processing step. In addition, the predicted longitudinal phase-space is blurry and has significant artifacts in the background. Moreover, the current profile was predicted by using another multi-layer perception instead of extracted directly from the predicted longitudinal phase-space. Indeed, a multi-layer perception consisting of purely fully connected layers has intrinsic limitations in image-related tasks as it intends to find the connection between each pair of nodes between each two adjacent layers. First of all, it unnecessarily complicates the training of the model as pixels representing the phase-space distribution apparently has no connection with majority of the background pixels. Secondly, the number of parameters scales quadratically with the number of pixels in the image, which makes it impractical to be applied on megapixel images due to the huge

memory requirement.

## METHOD

The detailed structure of the proposed autoencoder is shown in Fig. 2. We use a multi-layer perception to learn latent features and then generate the image on the screen from the latent features using a concatenation of transposed convolutional layers [14]. The transposed convolutional layer performs the transformation in the opposite direction of a normal convolution, which projects localized feature maps to a higher-dimensional space. It should be noted that developing neural networks directly operating on megapixel images is not trivial due to computational and memory constraints. Many state of the art models can only operate on images with less than 100,000 pixels [15]. Nevertheless, the time consumption for a single prediction with our model is about 15 ms with a mid-range graphics card, which is still orders of magnitude faster than standard beam dynamics simulation.

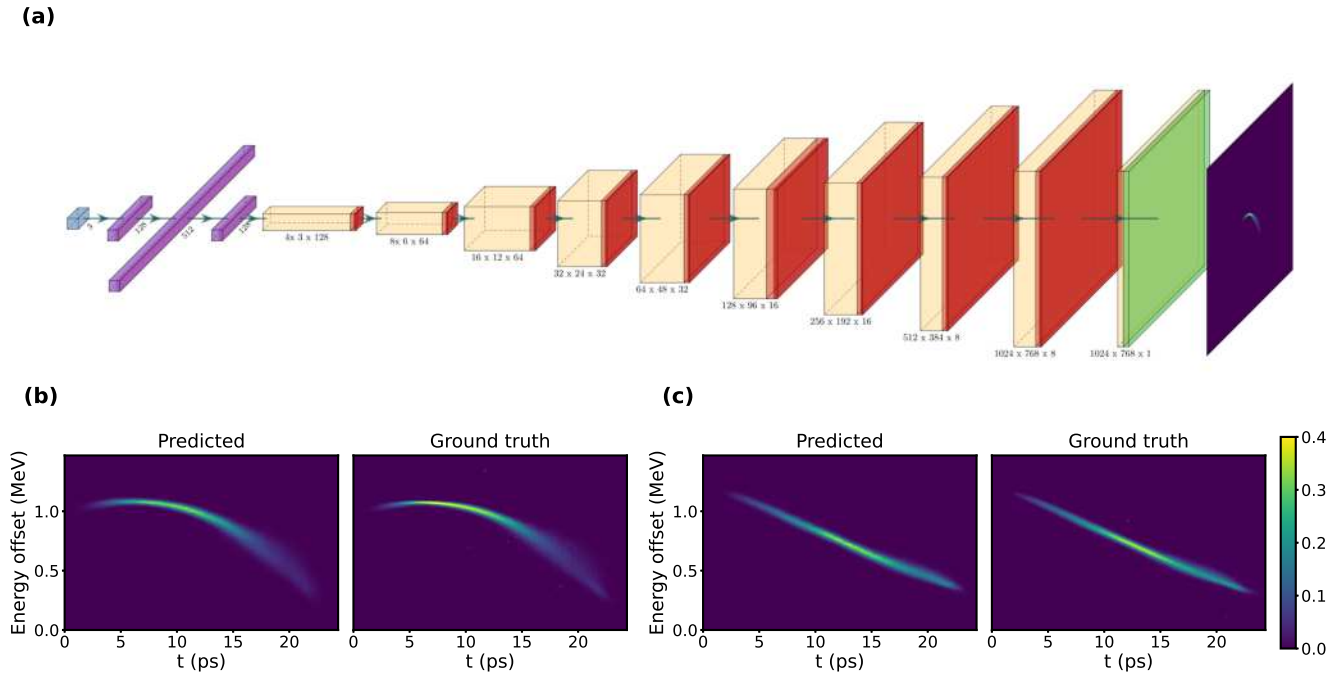


FIG. 2. (a) Diagram of the neural network. The leftmost blue box represents the input layer. It is followed by three fully-connected layers (encoder) in purple with each layer activated by the Leaky ReLU (Rectified Linear Unit) function. The ten yellow boxes present the transposed convolutional layers (decoder). Each transposed convolutional layer is followed by a batch normalization layer [16] and activated by the leaky ReLU function except the last one, which is activated by the sigmoid function depicted in green. The total number of parameters is 738,681. (b) First example of the longitudinal phase-spaces cropped from the predicted image and the corresponding ground truth. (c) Second example of the longitudinal phase-spaces cropped from the predicted image and the corresponding ground truth. The longitudinal phase-space is linearized by a third-harmonic linearizer cavity.

Neural networks are trained using the mini-batch

stochastic gradient decent optimization algorithm [16]

driven by a loss function. For most of the regression problems, the choice of the loss function defaults to mean squared error (MSE) [4–6]. However, MSE treats pixels as uncorrelated features and it was found that MSE results in an overly smoothed image and loss of high-frequency features in high-resolution image generation applications [17]. Structural similarity index measure (SSIM) [18] is another widely adopted metrics for image quality assessment which takes correlations of adjacent pixels into account. In our model, the loss of a mini-batch is given by

$$L_{batch} = \frac{1}{N_b} \sum_{i=1}^{N_b} (1 - f_{SSIM}(\mathbf{y}_i, \hat{\mathbf{y}}_i)), \quad (1)$$

where  $N_b$  the batch size for training,  $\hat{\mathbf{y}}$  the prediction and  $f_{SSIM}$  is SSIM in multiple scales written as

$$f_{SSIM}(\mathbf{y}, \hat{\mathbf{y}}) = l_M^{\alpha_M}(\mathbf{y}, \hat{\mathbf{y}}) \prod_{j=0}^M c_i^{\beta_j}(\mathbf{y}, \hat{\mathbf{y}}) s_j^{\gamma_j}(\mathbf{y}, \hat{\mathbf{y}}). \quad (2)$$

Here,  $l_j(\mathbf{y}, \hat{\mathbf{y}})$ ,  $c_j(\mathbf{y}, \hat{\mathbf{y}})$  and  $s_j(\mathbf{y}, \hat{\mathbf{y}})$  measure the distortions in luminance, contrast and structure [18], respectively, after scaling down the images by a factor of  $2^j$ . We empirically chose  $M = 2$  and  $\alpha_j = \beta_j = \gamma_j$  with  $\alpha_1 = 0.05$ ,  $\alpha_2 = 0.20$ ,  $\alpha_3 = 0.75$  for this study.

## EXPERIMENTAL RESULTS

The experiment was carried out at the injector of European XFEL [19] and the layout of the beamline is shown in Fig. 3. The nominal beam energy is 130 MeV which was measured at the maximum mean momentum gain (MMMG) phases of the gun and A1 as well as the zero-crossing [20] phase of AH1. We refer to this working point as the reference working point and the corresponding phases as reference phases. The bunch charge is around 250 pC. The TDS and the dipole magnet were used to measure the longitudinal phase-space at a resolution of about 0.047 ps/pixel and 0.0062 MeV/pixel. During the data collection, the phases of gun, A1 and AH1 were uniformly sampled within  $\pm 3$  degrees,  $\pm 6$  degrees and  $\pm 6$  degrees relative to the respective reference phases. It should be noted that the MMMG phase of A1 and the zero-crossing phase of AH1 change as the gun phase changes due to the time of flight change.

The original image size is 2330 x 1750 pixels. After background subtraction, all the negative pixel values were set to 0. To fit in the decoder network, the image was first cropped to 2048 x 1536 pixels at fixed positions. The cropped images are then downsampled by a factor of 2 to 1024 x 768 pixels in order to have a reasonable training time during our study with limited computational resources. For training, we adopted the weight initialization in [21] and Adam optimizer [22] with a fixed learning

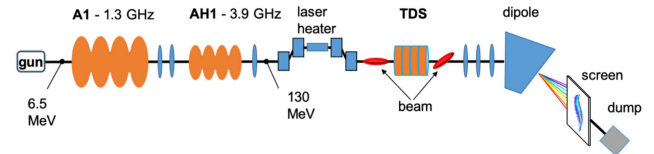


FIG. 3. Schematic of the European XFEL photoinjector and its diagnostic beamline. The phases of gun, A1 and AH1 were used as input to predict the image on the screen. The laser heater was switched off during the experiment.

rate of 3e-4 and the training was terminated after 600 epochs. In total, 3,000 shots were collected. 80% of the data were used for training and the rest were used for testing. In machine learning, it is critical that the information of the test data must not be used during training in order to avoid overfitting of the model. This could be a problem for randomly sampled data. Fig. 4(a) illustrates that there are enough distances between data points in our dataset. Moreover, Fig. 4(b-c) show that the distribution of pixel values are not centered for the image data.

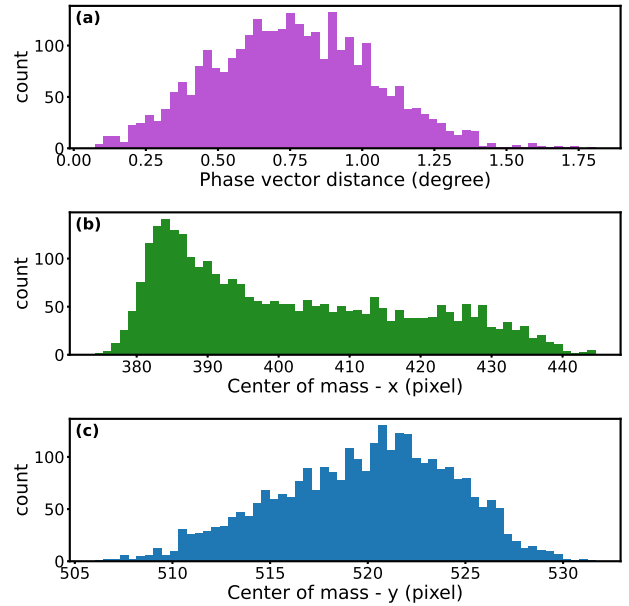


FIG. 4. Statistics of the whole dataset: (a) Histogram of the minimum Euclidean distance between the phase vector of each data point and the rest data. (b - c) Histograms of the x and y coordinates of the center of mass.

An example predicted image is shown in Fig. 5(b). It exhibits a very clean background. It must be pointed out that the ground truth image shown in Fig. 5(c) does have low-intensity background noise which is not visible with the current colormap. The predicted and ground truth longitudinal phase-spaces agree very well at different longitudinal positions of the bunch, which have expe-

rienced different non-linear forces while traveling through the beamline. We also trained another model to demonstrate the influence of the loss function. The second model has the same structure as the first one but uses MSE as the loss function. The result shown in Fig. 5(d) is apparently not as sharp as the phase-space shown in Fig. 5(b). The third model uses the same loss function as the first one but only has 6 transposed convolutional layers in the decoder. The predicted longitudinal phase-space shown in Fig. 5(e) contains obvious mesh-like structures. Fig. 5(f) further compares the current profiles extracted from Fig. 5(b-e). Evidently, the result from the first model has the best agreement with the ground truth.

In fact, the loss function used in training a machine learning model does not necessarily need to be the evaluation metrics of the model. Loss functions are often designed to be differentiable, and preferably convex and smooth, whereas many evaluation metrics are not [23]. The multi-scale SSIM given by Eq. 2 is calculated to be as high as  $\sim 0.997$  on the whole test dataset for all the above three models, which actually differ considerably in performance. Moreover, it can be difficult to find a proper evaluation metrics for applications like longitudinal phase-space prediction.

## TRANSFER LEARNING

Standard accelerator codes simulate the beam transport through each component along a beamline in a sequential order, which makes it easy to re-use part of the simulation result. Although the deep learning model used in this study takes the whole beamline for a single component, it is possible to leverage the trained model in other beamline setups. This is also called transfer learning in machine learning methodologies [24]. One of the most frequently used approach in transfer learning is to fine-tune the weights of a trained model for a new task. To demonstrate this, we recorded another 3,000 data points with a different setup of the injector. In the new setup, AH1 was switched off and the gradient of A1 was reduced accordingly to keep the nominal beam energy at 130 MeV. All the other beamline components remain the same as before. We trained the model on the new dataset using two approaches: continue training with the previous trained model and training from scratch. The learning curves are shown in Fig. 6(a). It is apparent that the training converges much faster with transfer learning. The predicted longitudinal phase-space, current profile and RMS slice energy spread all agree very well with the ground truth values, as shown in Fig. 6(b-d).

As accelerator operations suffer from long-term drift, a deep learning model may need to be re-trained from time to time with new data. Transfer learning has the potential to significantly reduce the time for the routine training. In addition, for a model with multiple decoders

for different diagnostics, one can freeze the weights in the encoder and train a new decoder for a newly added diagnostics, which is another commonly used approach in transfer learning [24].

## DISCUSSION AND OUTLOOK

In this study, we exploit the expressiveness of deep neural networks to model the longitudinal diagnostic beamline at the European XFEL photoinjector. The deep learning-based autoencoder model trained only with the experimental data is capable of precisely predicting megapixel images which are used for longitudinal phase-space measurement. The longitudinal phase-space extracted from the predicted image agrees very well with the ground truth not only visually, but also in important physical properties such as the current profile and the slice energy spread. The performance of the model could be further improved through a comprehensive hyperparameter tuning. Looking forward, more decoders for other diagnostics can be attached to the same encoder to enable a more complete model of the photoinjector using this data-driven approach.

We expect the autoencoder architecture to be applied to many other image-based beam diagnostics, not only for accelerators but also for the user photon beamlines, since we have not made any assumption on longitudinal phase-space while building and training the model. From another point of view, this inspires us to further improve the performance of the model by guiding it to focus on learning specific features from a longitudinal phase-space in the future study.

---

- [1] W. Decking and et al., A mhz-repetition-rate hard x-ray free-electron laser driven by a superconducting linear accelerator, *Nat. Photonics* **14**, 391 (2020).
- [2] S. Pascarelli, S. Molodtsov, and T. Tschentscher, Creating a diverse international user facility., *Nat. Rev. Phys.* **2**, 337 (2020).
- [3] A. Sanchez-Gonzalez and et al., Accurate prediction of x-ray pulse properties from a free-electron laser using machine learning, *Nat. Commun.* **8**, 15461 (2017).
- [4] C. Emma, A. Edelen, M. Hogan, B. O'Shea, G. White, and V. Yakimenko, Machine learning-based longitudinal phase space prediction of particle accelerators, *Phys. Rev. Accel. Beams* **21**, 112802 (2018).
- [5] A. Edelen, N. Neveu, M. Frey, Y. Huber, C. Mayes, , and A. Adelmann, Machine learning for orders of magnitude speedup in multiobjective optimization of particle accelerator systems, *Phys. Rev. Accel. Beams* **23**, 044601 (2020).
- [6] X. Ren, A. Edelen, A. Lutman, G. Marcus, T. Maxwell, , and D. Ratner, Temporal power reconstruction for an x-ray free-electron laser using convolutional neural networks, *Phys. Rev. Accel. Beams* **23**, 040701 (2020).

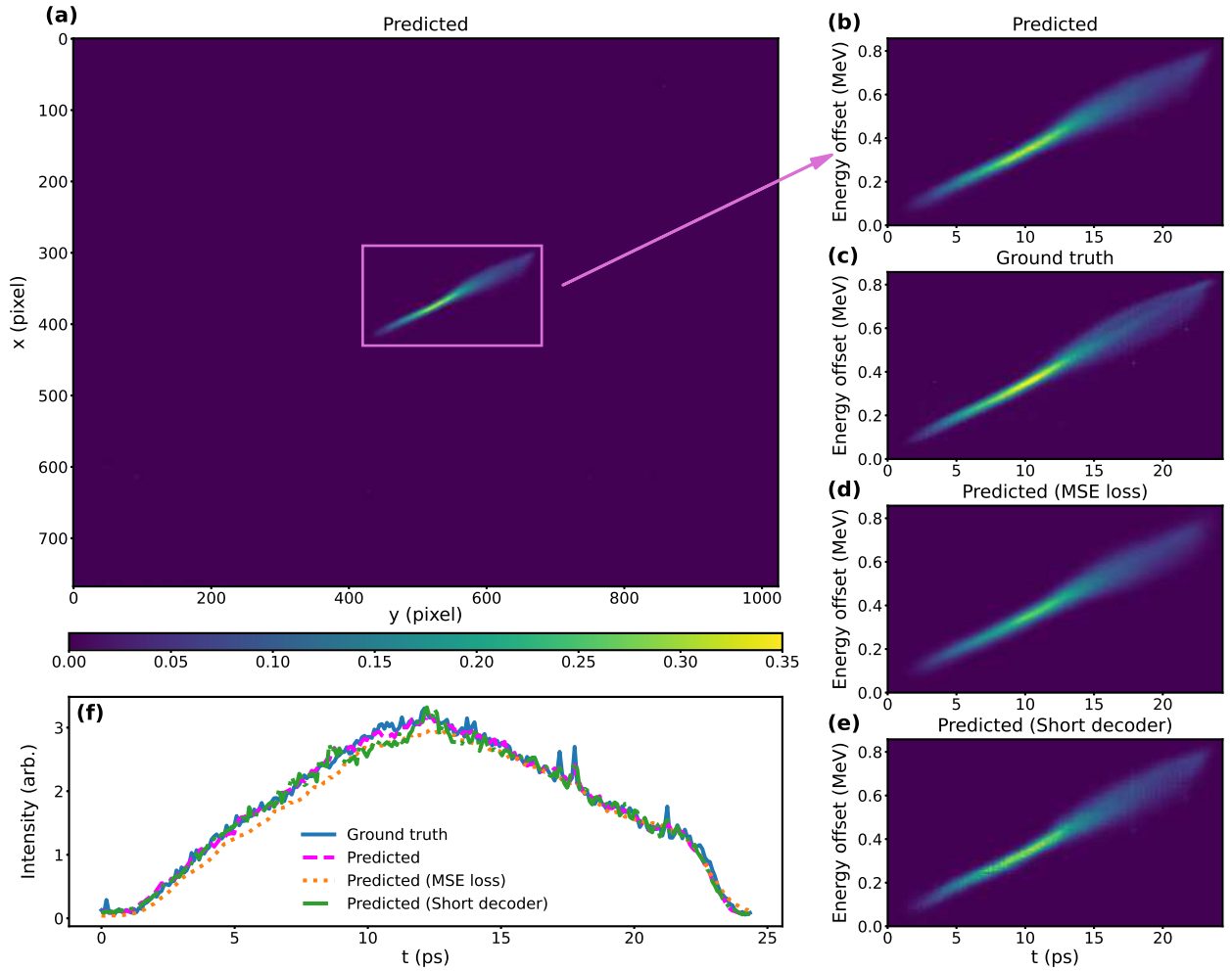


FIG. 5. (a) Example of an entire predicted image. The image is rotated by 90 degree. The relative phases of gun, A1 and AH1 are -1.17 degree, -1.38 degree and 0.04 degree, respectively. (b) Longitudinal phase-space cropped from the predicted image. (c) Longitudinal phase-space cropped from the ground truth image. (d) Longitudinal phase-space cropped from the image predicted by a model with the same structure but using MSE as the loss function. (e) Longitudinal phase-space cropped from the image predicted by a model with only 6 layers in the decoder. (f) Projections of pixel values along the y-axis for the predictions and the ground truth shown in (b-e).

- [7] A. Scheinker, A. Edelen, D. Bohler, C. Emma, and A. Lutman, Demonstration of model-independent control of the longitudinal phase space of electron beams in the linac-coherent light source with femtosecond resolution, *Phys. Rev. Lett.* **121**, 044801 (2018).
- [8] C. Emma, A. Edelen, A. Hanuk, B. O'Shea, and A. Scheinker, Virtual diagnostic suite for electron beam prediction and control, *Preprints* 2021, 2021010115.
- [9] N. A. Moody and et al., Perspectives on designer photocathodes for x-ray free-electron lasers: influencing emission properties with heterostructures and nanoengineering electronic states, *Phys. Rev. Applied* **10**, 047002 (2018).
- [10] Y. Chen, I. Zagorodnov, and M. Dohlus, Beam dynamics of realistic bunches at the injector section of the european x-ray free-electron laser, *Phys. Rev. Accel. Beams* **23**, 044201 (2020).
- [11] J. Qiang, Y. Ding, P. Emma, Z. Huang, D. Ratner, T. Raubenheimer, M. Venturini, and F. Zhou, Start-to-end simulation of the shot-noise driven microbunching instability experiment at the linac coherent light source, *Phys. Rev. Accel. Beams* **20**, 054402 (2017).
- [12] D. P. Kingma and M. Welling, An introduction to variational autoencoders, *Foundations and Trends® in Machine Learning* **12**, 307 (2019).
- [13] I. Goodfellow, J. Pouget-Abadie, M. Mirza, B. Xu, D. Warde-Farley, S. Ozair, A. Courville, and Y. Bengio, Generative adversarial networks, *arXiv:1406.2661*.
- [14] V. Dumoulin and F. Visin, A guide to convolution arithmetic for deep learning, *arXiv:1603.07285v2*.
- [15] A. Khan, A. Sohail, U. Zahoor, and A. S. Qureshi, A survey of the recent architectures of deep convolutional neural networks, *Artif. Intell. Rev.* **53**, 5455 (2020).
- [16] I. Goodfellow, Y. Bengio, and A. Courville, *Deep Learning* (MIT Press, 2016) <http://www.deeplearningbook.org>.

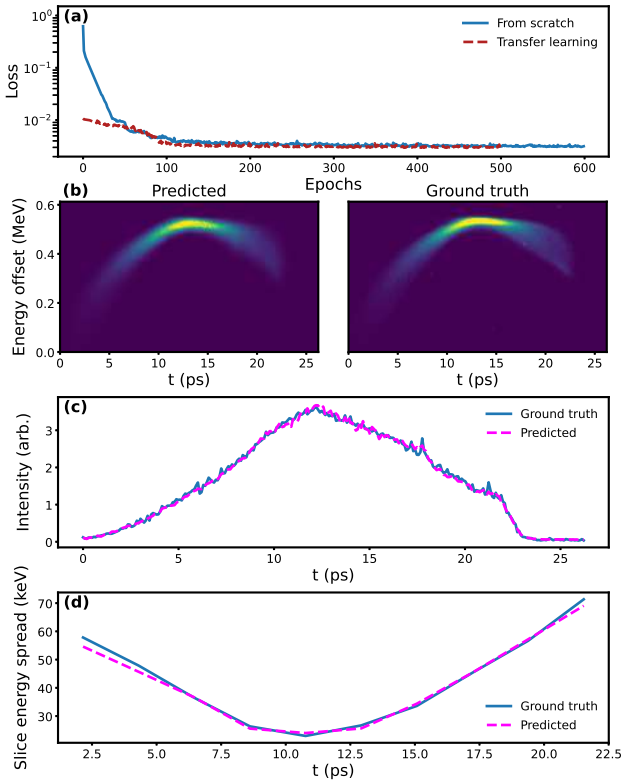


FIG. 6. (a) Learning curves for employing transfer learning and learning from scratch. (b) Example of predicted and ground truth longitudinal phase-spaces. The model was trained based on the model used in Fig. 5. The gun and A1 phases are -2.60 degree and 0.20 degree, respectively. (c) Projections of pixel values along the y-axis for the prediction and the ground truth shown in (b). (d) RMS slice energy spreads along the bunch for the prediction and the ground truth shown in (b).

- [17] C. Ledig, L. Theis, F. Huszár, J. Caballero, A. Cunningham, A. Acosta, A. Aitken, A. Tejani, J. Totz, Z. Wang, and W. Shi, Photo-realistic single image super-resolution using a generative adversarial network, in *2017 IEEE Conference on Computer Vision and Pattern Recognition (CVPR)* (2017) pp. 105–114.
- [18] Z. Wang, A. Bovik, H. Sheikh, and E. Simoncelli, Image quality assessment: From error visibility to structural similarity, *IEEE Trans. Image Process.* **13**, 600 (2004).
- [19] F. Brinker, Commissioning of the European XFEL Injector, in *7th International Particle Accelerator Conference* (2016) p. TUOCA03.
- [20] R. Akre, L. Bentson, P. Emma, and P. Krejcik, A transverse rf deflecting structure for bunch length and phase space diagnostics, in *PACS2001. Proceedings of the 2001 Particle Accelerator Conference* Vol. 3 (2001) pp. 2353–2355 vol.3.
- [21] K. He, X. Zhang, S. Ren, and J. Sun, Delving deep into rectifiers: Surpassing human-level performance on imagenet classification, in *2015 IEEE International Conference on Computer Vision (ICCV)* (2015) pp. 1026–1034.
- [22] J. B. Diederik P. Kingma, Adam: A method for stochastic optimization, arXiv:1412.6980.
- [23] C. Huang, S. Zhai, W. Talbott, M. B. Martin, S.-Y. Sun, C. Guestrin, and J. Susskind, Addressing the loss-metric mismatch with adaptive loss alignment, in *Proceedings of the 36th International Conference on Machine Learning* Proceedings of Machine Learning Research, Vol. 97, edited by K. Chaudhuri and R. Salakhutdinov (PMLR, 2019) pp. 2891–2900.
- [24] F. Zhuang, Z. Qi, K. Duan, D. Xi, Y. Zhu, H. Zhu, H. Xiong, and Q. He, A comprehensive survey on transfer learning, *Proceedings of the IEEE* **109**, 43 (2021).